# Antenna Correlation Under Geometry-Based Stochastic Channel Models

Yilin Ji, Wei Fan, Pekka Kyösti, Jinxing Li, and Gert Frølund Pedersen

***Abstract*—Antenna correlation is an important measure for designing multiple-input multiple-output (MIMO) antenna systems. A lower antenna correlation indicates a better MIMO performance that can be achieved with the underlying antenna systems. In the antenna design community, it is very common to evaluate the antenna correlation with isotropic or non-isotropic (e.g. Gaussian-distributed) angular power spectrum (APS) as baselines. On the other hand, antenna correlation can also be evaluated via channel transfer function (CTF) under the a given propagation channel, e.g. drawn from the bi-directional geometry-based stochastic channel model. In this paper, the analytic forms for the antenna correlation based on the APS and the CTF are derived, respectively, with their similarities and differences explained. Moreover, a numerical example is also given with a standard channel model to support our findings.**

***Index Terms*—MIMO, antenna correlation, GSCM models, spread function, angular power spectrum.**

## I. Introduction

Antenna correlation (also known as envelope correlation if absolute-squared) is widely used as a measure in both the antenna field and the propagation field for multiple-input multiple-output (MIMO) communications. It shows how much the received signals at different antenna ports correlate with each other. A lower antenna correlation indicates that a better performance can be expected for MIMO communications.

Without loss of generality, if we take the antenna correlation on the receive (Rx) side for example, the Rx antenna correlation can be analytically calculated with arbitrary incident angular power spectrum (APS) and Rx antenna field pattern [1]–[3]. It is very common in the antenna design community to evaluate the antenna correlation with some simplified channel models such as APS following the isotropic or non-isotropic (e.g. Gaussian or Laplacian) distributions as baselines [4].

On the other hand, Rx antenna correlation can also be calculated with another fundamental approach, i.e. through the cross correlation of the received signals at Rx antennas [5], [6]. This approach requires the knowledge of the channel transfer function (CTF) which describes the input-output relation between the transmit (Tx) and the Rx antenna ports of a communication system under a given propagation channel. However, not only the Rx antenna radiation pattern but also the Tx antenna radiation pattern are inherently embedded in the CTF, whereas the APS only describes the pure channel spatial characteristics with the Tx and Rx antenna radiation pattern de-embedded. Therefore, there might be some discrepancy between the two approaches introduced by the additional Tx antenna spatial selectivity in the second approach. Straightforwardly, stronger Tx antenna spatial selectivity, e.g. the fifth-generation (5G) base stations operating in beam forming modes, potentially alters the effective APS observed on the Rx side more severely, and hence leads to a more pronounced inconsistency between the two Rx antenna correlation approaches.

In this paper, we go through the derivation of the two antenna correlation approaches from APS and CTF, respectively. Both the two approaches are evaluated under the geometry-based stochastic channel model (GSCM), which has been developed in the propagation field and adopted in the standard [5], [7], [8], and the analytic form of the antenna correlation under the GSCM model is given explicitly. The connection between the two approaches is built through the spread function [9]. The difference between the end results of the antenna correlation from the two approaches are clarified, which shows the effect of the Tx antenna spatial selectivity on the resulting Rx correlation with the CTF approach. Finally, a numerical example is given with a standard channel model [5]. The main contribution of this paper is to bridge the gap between the two approaches via both theoretical analysis and numerical simulation, which has not been reported in the literature to our best knowledge.

The notations used in the paper are summarized as follow: $(\cdot)^{\mathrm{T}}$, $(\cdot)^*$, $|\cdot|$, and $\odot$ are the transpose, the complex conjugate, the absolute value, and the Hadamard product operator, respectively. Moreover, $cov\{\cdot,\cdot\}$, $var\{\cdot\}$, and $\mathbb{E}\{\cdot\}$ are the covariance, variance, and expectation operator, respectively.

## II. Propagation Channel Model

### A. Channel Transfer Function

The propagation channel is usually modelled as the superposition of a number of paths. For a MIMO system consisting of $S$ Tx antennas and $U$ Rx antennas, the CTF from the $s$th Tx antenna to the $u$th Rx antenna at time $t$ and frequency $f$ can be expressed as [9]

$$\begin{aligned} &H_{u,s}(t,f) \\ &= \iiiint \begin{bmatrix} F_s^{\mathrm{V}}(\boldsymbol{\Omega}^{\mathrm{Tx}}) \\ F_s^{\mathrm{H}}(\boldsymbol{\Omega}^{\mathrm{Tx}}) \end{bmatrix}^{\mathrm{T}} \boldsymbol{h}(\tau,\upsilon,\boldsymbol{\Omega}^{\mathrm{Tx}},\boldsymbol{\Omega}^{\mathrm{Rx}}) \begin{bmatrix} F_u^{\mathrm{V}}(\boldsymbol{\Omega}^{\mathrm{Rx}}) \\ F_u^{\mathrm{H}}(\boldsymbol{\Omega}^{\mathrm{Rx}}) \end{bmatrix} \\ &\quad \cdot \exp(j2\pi\upsilon t) \cdot \exp(-j2\pi f\tau)\,\mathrm{d}\tau\,\mathrm{d}\upsilon\,\mathrm{d}\boldsymbol{\Omega}^{\mathrm{Tx}}\,\mathrm{d}\boldsymbol{\Omega}^{\mathrm{Rx}}, \end{aligned} \tag{1}$$

where $\tau, \upsilon, \boldsymbol{\Omega}^{\mathrm{Tx}}, \boldsymbol{\Omega}^{\mathrm{Rx}}$ are the domains of delay, Doppler frequency, direction of departure (DoD), direction of arrival

Yilin Ji, Wei Fan, and Gert Frølund Pedersen are with Antenna Propagation and Millimeter-wave Systems (APMS) section at Department of Electronic Systems, Aalborg University, Denmark. (Corresponding author: Wei Fan. Email: wfa@es.aau.dk)

Pekka Kyösti is with University of Oulu, Finland, and with Keysight Technologies Finland oy, Finland.

Jinxing Li is with Huawei Technologies Co., Ltd.

(DoA), respectively. $F_s^{\mathrm{V}}(\mathbf{\Omega})$ and $F_s^{\mathrm{H}}(\mathbf{\Omega})$ are the antenna field patterns of the $s$th Tx antenna at direction $\mathbf{\Omega}$ for vertical polarization (V-pol) and horizontal polarization (H-pol), respectively. Similarly, $F_u^{\mathrm{V}}(\mathbf{\Omega})$ and $F_u^{\mathrm{H}}(\mathbf{\Omega})$ are those for the $u$th Rx antenna. The antenna field pattern is defined with a common phase center for the respective Tx and Rx antenna arrays. The integration is conducted over the full span of the respective domains.

In (1), the matrix $\boldsymbol{h}$ is the so-called spread function [9], and within the context of the GSCM models it can be written as

$$\boldsymbol{h}(\tau,\upsilon,\mathbf{\Omega}^{\mathrm{Tx}},\mathbf{\Omega}^{\mathrm{Rx}}) = \sum_{m=1}^{M} \sqrt{P_m}\cdot\boldsymbol{A}\cdot\delta(\tau-\tau_m)\cdot\delta(\upsilon-\upsilon_m) \cdot\delta(\mathbf{\Omega}^{\mathrm{Tx}}-\mathbf{\Omega}_m^{\mathrm{Tx}})\cdot\delta(\mathbf{\Omega}^{\mathrm{Rx}}-\mathbf{\Omega}_m^{\mathrm{Rx}}), \quad (2)$$

where $M$ is the number of paths, $P_m$ is the power of the $m$th path, $\tau_m,\upsilon_m,\mathbf{\Omega}_m^{\mathrm{Tx}},\mathbf{\Omega}_m^{\mathrm{Rx}}$ are the parameters of the $m$th path in their respective domains, and $\delta(\cdot)$ is the Dirac delta function. The matrix $\boldsymbol{A}$ is the polarization matrix

$$\boldsymbol{A} = \begin{bmatrix} \exp(j\Phi_m^{\mathrm{VV}}) & \sqrt{\kappa_{1,m}^{-1}}\exp(j\Phi_m^{\mathrm{VH}}) \\ \sqrt{\kappa_{2,m}^{-1}\chi_m^{-1}}\exp(j\Phi_m^{\mathrm{HV}}) & \sqrt{\chi_m^{-1}}\exp(j\Phi_m^{\mathrm{HH}}) \end{bmatrix}, \quad (3)$$

where

- $\Phi_m^{\mathrm{VV}}$, $\Phi_m^{\mathrm{VH}}$, $\Phi_m^{\mathrm{HV}}$, and $\Phi_m^{\mathrm{HH}}$ are the initial phases of the $m$th path of vertical-to-vertical (VV-pol), vertical-to-horizontal (VH-pol), horizontal-to-vertical (HV-pol), and horizontal-to-horizontal (HH-pol) polarizations, respectively. They are assumed independent and identically distributed (i.i.d.) random variables following the uniform distribution over $[0, 2\pi]$.
- $\kappa_{1,m}$ and $\kappa_{2,m}$ are the cross-polarization ratios (XPR) of the $m$th path, where $\kappa_{1,m}$ is the power ratio of VV-pol over VH-pol, and $\kappa_{2,m}$ HH-pol over HV-pol. It is usually assumed $\kappa_{1,m}=\kappa_{2,m}=\kappa_m$.
- $\chi_m$ is the co-polarization ratio (CPR) of the $m$th path defined as the power ratio of VV-pol over HH-pol.

Inserting (2) and (3) into (1) yields

$$H_{u,s}(t,f) = \sum_{m=1}^{M}\sqrt{P_m}\begin{bmatrix}F_s^{\mathrm{V}}(\mathbf{\Omega}_m^{\mathrm{Tx}})\\F_s^{\mathrm{H}}(\mathbf{\Omega}_m^{\mathrm{Tx}})\end{bmatrix}^{\mathrm{T}}\mathbf{A}\begin{bmatrix}F_u^{\mathrm{V}}(\mathbf{\Omega}_m^{\mathrm{Rx}})\\F_u^{\mathrm{H}}(\mathbf{\Omega}_m^{\mathrm{Rx}})\end{bmatrix} \cdot\exp(j2\pi\upsilon_m t)\cdot\exp(-j2\pi f\tau_m). \quad (4)$$

For brevity, in the following we abbreviate some of the notation as: $H_{u,s}(t,f)=H_{u,s}$; $F_s^{\mathrm{V}}(\mathbf{\Omega}_m^{\mathrm{Tx}})=F_{s,m}^{\mathrm{V}}$; $F_s^{\mathrm{H}}(\mathbf{\Omega}_m^{\mathrm{Tx}})=F_{s,m}^{\mathrm{H}}$; $F_u^{\mathrm{V}}(\mathbf{\Omega}_m^{\mathrm{Rx}})=F_{u,m}^{\mathrm{V}}$; $F_u^{\mathrm{H}}(\mathbf{\Omega}_m^{\mathrm{Rx}})=F_{u,m,}^{\mathrm{H}}$.

### *B. Angular Power Spectrum Derived from Spread Function*

The joint delay-Doppler-DoD-DoA power spectrum can be derived from the spread function as [9]

$$\boldsymbol{P}(\tau,\upsilon,\mathbf{\Omega}^{\mathrm{Tx}},\mathbf{\Omega}^{\mathrm{Rx}}) = \mathbb{E}\left\{\boldsymbol{h}(\tau,\upsilon,\mathbf{\Omega}^{\mathrm{Tx}},\mathbf{\Omega}^{\mathrm{Rx}})\odot\boldsymbol{h}(\tau,\upsilon,\mathbf{\Omega}^{\mathrm{Tx}},\mathbf{\Omega}^{\mathrm{Rx}})^*\right\}. \quad (5)$$

Inserting (2) into (5), and defining $|\delta(x)|^2 \doteq \delta(x)$ with $x$ being the dummy variable, we can obtain

$$\boldsymbol{P}(\tau,\upsilon,\mathbf{\Omega}^{\mathrm{Tx}},\mathbf{\Omega}^{\mathrm{Rx}}) = \sum_{m=1}^{M} P_m\cdot\overline{\boldsymbol{A}^2}\cdot\delta(\tau-\tau_m)\cdot\delta(\upsilon-\upsilon_m) \cdot\delta(\mathbf{\Omega}^{\mathrm{Tx}}-\mathbf{\Omega}_m^{\mathrm{Tx}})\cdot\delta(\mathbf{\Omega}^{\mathrm{Rx}}-\mathbf{\Omega}_m^{\mathrm{Rx}}), \quad (6)$$

where

$$\overline{\boldsymbol{A}^2} = \mathbb{E}\left\{\boldsymbol{A}\odot\boldsymbol{A}^*\right\} = \begin{bmatrix}1 & \kappa_m^{-1}\\ \kappa_m^{-1}\chi_m^{-1} & \chi_m^{-1}\end{bmatrix}, \quad (7)$$

using the i.i.d. property of the initial phases of the paths [10].

Conventionally, power spectrum is considered as a property of propagation channels, and it is independent on the antennas used on both the Tx and the Rx. In other words, the antenna pattern is de-embedded from the channel. It follows that the power spectrum in one (either marginal or joint) domain can be obtained by integrating the joint power spectrum of higher dimensions over the remaining domains [9]. Therefore, the joint DoD-DoA power spectrum can be derived as

$$\begin{aligned}\boldsymbol{P}(\mathbf{\Omega}^{\mathrm{Tx}},\mathbf{\Omega}^{\mathrm{Rx}}) &= \iint \boldsymbol{P}(\tau,\upsilon,\mathbf{\Omega}^{\mathrm{Tx}},\mathbf{\Omega}^{\mathrm{Rx}})\,\mathrm{d}\tau\,\mathrm{d}\upsilon \\ &= \sum_{m=1}^{M} P_m\cdot\overline{\boldsymbol{A}^2}\cdot\delta(\mathbf{\Omega}^{\mathrm{Tx}}-\mathbf{\Omega}_m^{\mathrm{Tx}})\cdot\delta(\mathbf{\Omega}^{\mathrm{Rx}}-\mathbf{\Omega}_m^{\mathrm{Rx}}),\end{aligned} \quad (8)$$

which is a $2\times 2$ matrix with the polarization relation between the Tx and the Rx described in $\overline{\boldsymbol{A}^2}$.

The power spectrum in the DoA domain can be further derived in a similar way as

$$\boldsymbol{P}(\mathbf{\Omega}^{\mathrm{Rx}}) = \int\begin{bmatrix}1\\1\end{bmatrix}^{\mathrm{T}}\boldsymbol{P}(\mathbf{\Omega}^{\mathrm{Tx}},\mathbf{\Omega}^{\mathrm{Rx}})\,\mathrm{d}\mathbf{\Omega}^{\mathrm{Tx}}, \quad (9)$$

where the vector of ones describes the antenna de-embedding assumption, and merges the V-pol and H-pol contribution from the Tx side. Inserting (8) into (9), $\boldsymbol{P}(\mathbf{\Omega}^{\mathrm{Rx}})$ can be explicitly expressed in both polarizations as

$$\boldsymbol{P}(\mathbf{\Omega}^{\mathrm{Rx}}) = \begin{bmatrix}P^{\mathrm{V}}(\mathbf{\Omega}^{\mathrm{Rx}})\\P^{\mathrm{H}}(\mathbf{\Omega}^{\mathrm{Rx}})\end{bmatrix}^{\mathrm{T}}, \quad (10)$$

where

$$P^{\mathrm{V}}(\mathbf{\Omega}^{\mathrm{Rx}}) = \sum_{m=1}^{M} P_m\cdot(1+\kappa_m^{-1}\chi_m^{-1})\cdot\delta(\mathbf{\Omega}^{\mathrm{Rx}}-\mathbf{\Omega}_m^{\mathrm{Rx}}), \quad (11a)$$

$$P^{\mathrm{H}}(\mathbf{\Omega}^{\mathrm{Rx}}) = \sum_{m=1}^{M} P_m\cdot(\kappa_m^{-1}+\chi_m^{-1})\cdot\delta(\mathbf{\Omega}^{\mathrm{Rx}}-\mathbf{\Omega}_m^{\mathrm{Rx}}). \quad (11b)$$

In many GSCM models [5], [7], [8], it is often assumed the CPR $\chi_m=1$, which leads to $P^{\mathrm{V}}(\mathbf{\Omega}^{\mathrm{Rx}})=P^{\mathrm{H}}(\mathbf{\Omega}^{\mathrm{Rx}})$.

## III. Antenna Correlation

### *A. Antenna Correlation from Channel Transfer Function*

The antenna correlation between two Rx antenna $u_1$ and $u_2$ can be calculated as [5], [6]

$$\rho_{u_1,u_2}^{\mathrm{CTF}} = \frac{cov\{H_{u_1,s},H_{u_2,s}\}}{\sqrt{var\{H_{u_1,s}\}}\cdot\sqrt{var\{H_{u_2,s}\}}}. \quad (12)$$

Inserting (3) and (4) into (12), and using the i.i.d. property of the initial phases of the paths [10], it yields

$$\rho^{\text{CTF}}_{u_1,u_2} = \frac{\beta_{u_1,u_2}}{\sqrt{\beta_{u_1}} \cdot \sqrt{\beta_{u_2}}}, \tag{13}$$

where

$$\begin{aligned}\beta_{u_1,u_2} &= \sum_{m=1}^{M} \Big\{ P_m(|F^{\text{V}}_{s,m}|^2 + \kappa_m^{-1}\chi_m^{-1}|F^{\text{H}}_{s,m}|^2) \cdot F^{\text{V}}_{u_1,m} \cdot F^{\text{V}*}_{u_2,m} \\ &\quad + P_m(\kappa_m^{-1}|F^{\text{V}}_{s,m}|^2 + \chi_m^{-1}|F^{\text{H}}_{s,m}|^2) \cdot F^{\text{H}}_{u_1,m} \cdot F^{\text{H}*}_{u_2,m} \Big\}, \quad (14a)\\ \beta_u &= \sum_{m=1}^{M} \Big\{ P_m(|F^{\text{V}}_{s,m}|^2 + \kappa_m^{-1}\chi_m^{-1}|F^{\text{H}}_{s,m}|^2) \cdot |F^{\text{V}}_{u,m}|^2 \\ &\quad + P_m(\kappa_m^{-1}|F^{\text{V}}_{s,m}|^2 + \chi_m^{-1}|F^{\text{H}}_{s,m}|^2) \cdot |F^{\text{H}}_{u,m}|^2 \Big\}. \quad (14b)\end{aligned}$$

### *B. Antenna Correlation from Angular Power Spectrum*

The antenna correlation between two Rx antennas, $u_1$ and $u_2$, can also be calculated as [1] (c.f. (13))

$$\rho^{\text{APS}}_{u_1,u_2} = \frac{\gamma_{u_1,u_2}}{\sqrt{\gamma_{u_1}} \cdot \sqrt{\gamma_{u_2}}}, \tag{15}$$

where

$$\begin{aligned}\gamma_{u_1,u_2} &= \int \Big\{ \eta \cdot p^{\text{V}}(\boldsymbol{\Omega}^{\text{Rx}}) \cdot F^{\text{V}}_{u_1}(\boldsymbol{\Omega}^{\text{Rx}}) \cdot F^{\text{V}}_{u_2}(\boldsymbol{\Omega}^{\text{Rx}})^* \\ &\quad + p^{\text{H}}(\boldsymbol{\Omega}^{\text{Rx}}) \cdot F^{\text{H}}_{u_1}(\boldsymbol{\Omega}^{\text{Rx}}) \cdot F^{\text{H}}_{u_2}(\boldsymbol{\Omega}^{\text{Rx}})^* \Big\} \, \mathrm{d}\boldsymbol{\Omega}^{\text{Rx}}, \quad (16a)\\ \gamma_u &= \int \Big\{ \eta \cdot p^{\text{V}}(\boldsymbol{\Omega}^{\text{Rx}}) \cdot |F^{\text{V}}_{u}(\boldsymbol{\Omega}^{\text{Rx}})|^2 \\ &\quad + p^{\text{H}}(\boldsymbol{\Omega}^{\text{Rx}}) \cdot |F^{\text{H}}_{u}(\boldsymbol{\Omega}^{\text{Rx}})|^2 \Big\} \, \mathrm{d}\boldsymbol{\Omega}^{\text{Rx}}, \quad (16b)\end{aligned}$$

with $p^{\text{V}}(\boldsymbol{\Omega}^{\text{Rx}})$ and $p^{\text{H}}(\boldsymbol{\Omega}^{\text{Rx}})$ being the normalized APS, i.e. $\int p^{\text{V}}(\boldsymbol{\Omega}^{\text{Rx}}) \, \mathrm{d}\boldsymbol{\Omega}^{\text{Rx}} = \int p^{\text{H}}(\boldsymbol{\Omega}^{\text{Rx}}) \, \mathrm{d}\boldsymbol{\Omega}^{\text{Rx}} = 1$, in the DoA domain for V-pol and H-pol, respectively. The term $\eta$ is the so-called V/H ratio [5], and is defined as the ratio of the total power of the incident signal of the V-pol over that of the H-pol.

It must be noted that in the literature the V/H ratio is often termed also as XPR depending on the background, which is sometimes confusing to that defined in the GSCM model as described in Section II-A. Therefore, additional care shall be taken for those values in practice for calculation.

The normalized APS for both polarizations can be obtained with (11) as

$$p^{\text{V}}(\boldsymbol{\Omega}^{\text{Rx}}) = \frac{P^{\text{V}}(\boldsymbol{\Omega}^{\text{Rx}})}{P^{\text{V}}_{\text{tot}}}, \tag{17a}$$

$$p^{\text{H}}(\boldsymbol{\Omega}^{\text{Rx}}) = \frac{P^{\text{H}}(\boldsymbol{\Omega}^{\text{Rx}})}{P^{\text{H}}_{\text{tot}}}, \tag{17b}$$

with

$$P^{\text{V}}_{\text{tot}} = \sum_{m=1}^{M} P_m(1 + \kappa_m^{-1}\chi_m^{-1}), \tag{18a}$$

$$P^{\text{H}}_{\text{tot}} = \sum_{m=1}^{M} P_m(\kappa_m^{-1} + \chi_m^{-1}), \tag{18b}$$

being the total incident power for both polarizations. In addition, the V/H ratio $\eta$ can be obtained as

$$\eta = \frac{P^{\text{V}}_{\text{tot}}}{P^{\text{H}}_{\text{tot}}}. \tag{19}$$

Equation (19) also indicates the V/H ratio $\eta$ can be uniquely determined from the XPR $\kappa_m$ and CPR $\chi_m$ but not vice versa.

Inserting (17), (18), and (19) into (16) and with some equation manipulation, we can obtain the antenna correlation $\rho^{\text{APS}}_{u_1,u_2}$ under the same channel model as for $\rho^{\text{CTF}}_{u_1,u_2}$ as

$$\begin{aligned}\gamma_{u_1,u_2} &= \sum_{m=1}^{M} \Big\{ P_m(1 + \kappa_m^{-1}\chi_m^{-1}) \cdot F^{\text{V}}_{u_1,m} \cdot F^{\text{V}*}_{u_2,m} \\ &\quad + P_m(\kappa_m^{-1} + \chi_m^{-1}) \cdot F^{\text{H}}_{u_1,m} \cdot F^{\text{H}*}_{u_2,m} \Big\}, \quad (20a)\\ \gamma_u &= \sum_{m=1}^{M} \Big\{ P_m(1 + \kappa_m^{-1}\chi_m^{-1}) \cdot |F^{\text{V}}_{u,m}|^2 \\ &\quad + P_m(\kappa_m^{-1} + \chi_m^{-1}) \cdot |F^{\text{H}}_{u,m}|^2 \Big\}. \quad (20b)\end{aligned}$$

### *C. Relation Between the Two Antenna Correlation Approaches*

By comparing (14) and (20), we can find that the difference between $\rho^{\text{APS}}_{u_1,u_2}$ and $\rho^{\text{CTF}}_{u_1,u_2}$ is solely caused by the discrepancy of the antenna de-embedding assumption between the two approaches. Since the CTF describes the input-output relation between the Tx antenna ports and the Rx antenna ports, antenna pattern is not de-embedded from the CTF (1). Therefore, the effective power spectrum in the DoA domain for the CTF case accounting for the Tx antenna pattern can be alternatively formulated as (c.f. (9))

$$\widetilde{\boldsymbol{P}}(\boldsymbol{\Omega}^{\text{Rx}}) = \int \begin{bmatrix} |F^{\text{V}}_{s}(\boldsymbol{\Omega}^{\text{Tx}})|^2 \\ |F^{\text{H}}_{s}(\boldsymbol{\Omega}^{\text{Tx}})|^2 \end{bmatrix}^{\text{T}} \boldsymbol{P}(\boldsymbol{\Omega}^{\text{Tx}}, \boldsymbol{\Omega}^{\text{Rx}}) \, \mathrm{d}\boldsymbol{\Omega}^{\text{Tx}}. \tag{21}$$

If we derive the antenna correlation $\rho^{\text{APS}}_{u_1,u_2}$ with respect to $\widetilde{\boldsymbol{P}}(\boldsymbol{\Omega}^{\text{Rx}})$ following the same way in Section III-B, and denote that as $\widetilde{\rho}^{\text{APS}}_{u_1,u_2}$, it is very straightforward to find

$$\widetilde{\rho}^{\text{APS}}_{u_1,u_2} = \rho^{\text{CTF}}_{u_1,u_2}. \tag{22}$$

Alternatively, we can also consider $\rho^{\text{APS}}_{u_1,u_2}$ as a special case of $\rho^{\text{CTF}}_{u_1,u_2}$ with $|F^{\text{V}}_{s}(\boldsymbol{\Omega}^{\text{Tx}})|^2 = |F^{\text{H}}_{s}(\boldsymbol{\Omega}^{\text{Tx}})|^2 = 1$. Given clarification on the antenna de-embedding assumption for both approaches, the discrepancy can be resolved resulting in the same antenna correlation results.

Another interesting effect of the discrepancy is that since the effective APS $\widetilde{\boldsymbol{P}}(\boldsymbol{\Omega}^{\text{Rx}})$ is ruled by both the joint $\boldsymbol{P}(\boldsymbol{\Omega}^{\text{Tx}}, \boldsymbol{\Omega}^{\text{Rx}})$ and the Tx antenna pattern as shown in (21), the resulting $\rho^{\text{CTF}}_{u_1,u_2}$ becomes dependent on the joint $\boldsymbol{P}(\boldsymbol{\Omega}^{\text{Tx}}, \boldsymbol{\Omega}^{\text{Rx}})$ instead of just the marginal $\boldsymbol{P}(\boldsymbol{\Omega}^{\text{Rx}})$ as for $\rho^{\text{APS}}_{u_1,u_2}$. An intuitive example of this effect can be made by changing the pairing order between the DoD $\boldsymbol{\Omega}^{\text{Tx}}_m$ and the DoA $\boldsymbol{\Omega}^{\text{Rx}}_{m'}$ with $m, m' \in [1, M]$ in the channel according to [7]. Different pairing orders result in different joint $\boldsymbol{P}(\boldsymbol{\Omega}^{\text{Tx}}, \boldsymbol{\Omega}^{\text{Rx}})$, while the corresponding marginal $\boldsymbol{P}(\boldsymbol{\Omega}^{\text{Rx}})$ always remains the same. As a result, $\rho^{\text{APS}}_{u_1,u_2}$ remains unchanged, whereas $\rho^{\text{CTF}}_{u_1,u_2}$ changes with different joint $\boldsymbol{P}(\boldsymbol{\Omega}^{\text{Tx}}, \boldsymbol{\Omega}^{\text{Rx}})$ filtered by the Tx the spatial selectivity. Those findings show the effect of the Tx spatial selectivity on the resulting Rx antenna correlation with the CTF approach.

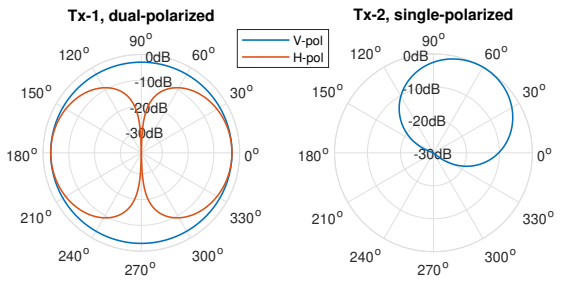


Fig. 1. The azimuth antenna pattern of (Tx-1) the 45° slanted ideal dipole [5], and (Tx-2) the V-pol dipole with 65° HPBW and boresight at 60° [7].

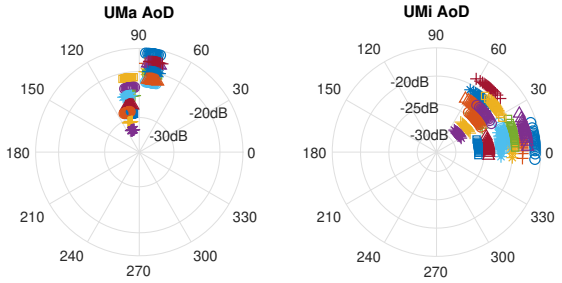


Fig. 2. The APS in the azimuth angle of departure (AoD) domain for (left) the SCME UMa scenario and (right) the SCME UMi scenario [5]. Colors and markers differ the 18 clusters and each cluster are modelled with 20 subpaths (denoted as scatterers).

## IV. Numerical Examples

In this section, we take the SCME Urban Macro-cell (UMa) and Urban Micro-cell (UMi) channel model [5] as the reference channels, and three configurations for the Tx antennas, to demonstrate the difference of the two antenna correlation approaches. Tx config-0 (Tx-0) is the case where the Tx antennas are de-embedded; Tx config-1 (Tx-1) is a 45° slanted ideal dipole with isotropic gain [5]; and Tx config-2 (Tx-2) is a V-pol dipole with 65° half-power beam width and boresight at 60° [7]. The corresponding Tx antenna pattern and APS in the azimuth plane are shown in Fig. 1 and Fig. 2, respectively.

The V/H ratio $\eta$ is calculated from $\widetilde{\boldsymbol{P}}(\boldsymbol{\Omega}^{\mathrm{Rx}})$ with the three Tx configurations. The resulting values are shown in Table I for both the UMa and UMi scenarios with the input parameters XPR $\kappa_m = 9\,\mathrm{dB}$ and CPR $\chi_m = 0\,\mathrm{dB}$ taken from the SCME model. The difference between the values of $\eta$ from different Tx configurations is significant. More specifically, the large V/H ratio for Tx-1 under the UMa scenario is caused by the polarization discrimination around 90° between the V-pol and H-pol Tx antenna pattern, where the AoDs of the paths happen to be located. When the Tx antenna is only V-pol as for Tx-2, the V/H ratio equals the XPR.

Further, the antenna correlation is calculated with isotropic antennas on the Rx side and shown in Fig. 3. The antenna spacing between the Rx antennas is swept from 0 to $2\lambda$ (wavelength), and the broadside of the two Rx antennas is aligned to 0° in the azimuth plane. The AoDs and the AoAs of the 20 subpaths of each cluster are first paired up randomly, and then the resulting pairing order is fixed throughout the simulation to have a fixed joint AoD-AoA power spectrum for a fair comparison of $\rho^{\mathrm{CTF}}_{u_1,u_2}$ with different Tx configurations.

TABLE I
The Effect of Tx Antenna Pattern on the Resulting V/H Ratio.

| | SCME UMa | | | SCME UMi | | |
|---|---|---|---|---|---|---|
| Tx Configs | $\kappa_m$ | $\chi_m$ | $\eta$ | $\kappa_m$ | $\chi_m$ | $\eta$ |
| Tx-0 | 9 dB | 0 dB | 0 dB | 9 dB | 0 dB | 0 dB |
| Tx-1 | 9 dB | 0 dB | 8.14 dB | 9 dB | 0 dB | 0.74 dB |
| Tx-2 | 9 dB | 0 dB | 9 dB | 9 dB | 0 dB | 9 dB |

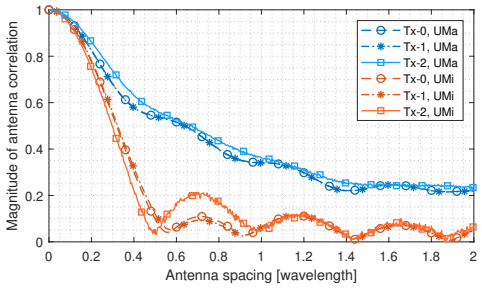


Fig. 3. The magnitude of the antenna correlation $\rho^{\mathrm{CTF}}_{u_1,u_2}$ against antenna spacing with the three Tx configurations under the UMa and the UMi channel. Note that $\rho^{\mathrm{CTF}}_{u_1,u_2}$ with Tx-0 is equivalent to $\rho^{\mathrm{APS}}_{u_1,u_2}$.

Note that $\rho^{\mathrm{CTF}}_{u_1,u_2}$ with Tx-0 is equivalent to $\rho^{\mathrm{APS}}_{u_1,u_2}$ as discussed in Section III-C.

We can see that difference between $\rho^{\mathrm{CTF}}_{u_1,u_2}$ and $\rho^{\mathrm{APS}}_{u_1,u_2}$ is more significant with Tx-2 than with Tx-1 for both scenarios. The reason is that the directional antenna pattern of Tx-2 alters $\widetilde{\boldsymbol{P}}(\boldsymbol{\Omega}^{\mathrm{Rx}})$ more severely than Tx-1 does. Moreover, the difference is more significant under the UMi scenario than under the UMa scenario for the same Tx configuration. This is because the larger AoD spread under the UMi scenario introduces more variation from the Tx antenna pattern to $\widetilde{\boldsymbol{P}}(\boldsymbol{\Omega}^{\mathrm{Rx}})$ compared to the UMa scenario. Therefore, we can expect that a more noticeable difference between $\rho^{\mathrm{CTF}}_{u_1,u_2}$ and $\rho^{\mathrm{APS}}_{u_1,u_2}$ may occur if either the AoD spread of a given channel is larger or the Tx antenna pattern is more directional.

## V. Conclusion

In this paper, we derived the analytic forms for the antenna correlation based on the CTF and the APS, respectively. The relation between the antenna correlation from the two approaches is described with the spread function. It is shown explicitly in the derivation that the difference between them is caused by the antenna de-embedding assumption made for the APS, which is not generally assumed for the CTF. It is also pointed out that the two antenna correlation approaches can be equivalent if the same assumption is made for the CTF.

Antenna correlation under the two approaches and V/H ratio are evaluated with the SCME UMa and UMi channel model as an example, which numerically shows the effect of the spatial selectivity of the Tx antennas on the results. The APS approach is generally adopted in the antenna community to calculate antenna correlation, which is a key measure to design MIMO antennas, and our theoretical analysis and numerical simulation show that ignoring Tx antenna pattern might lead to inaccurate Rx antenna correlation calculation with this approach.

## REFERENCES


[1] C. A. Balanis, *Antenna Theory: Analysis and Design*. John Wiley & Sons, 2005.

[2] R. Vaughan and J. B. Andersen, *Channels , Propagation and Antennas for Mobile Communications*. The Institution of Electrical Engineers, 2003.

[3] L. Schumacher, K. I. Pedersen, and P. E. Mogensen, "From antenna spacings to theoretical capacities - Guidelines for simulating MIMO systems," *IEEE International Symposium on Personal, Indoor and Mobile Radio Communications, PIMRC*, vol. 2, pp. 587–592, 2002.

[4] I. Szini, B. Yanakiev, and G. F. Pedersen, "MIMO reference antennas performance in anisotropic channel environments," *IEEE Transactions on Antennas and Propagation*, vol. 62, no. 6, pp. 3270–3280, 2014.

[5] 3GPP, "Verification of radiated multi-antenna reception performance of User Equipment (UE)," Technical Specification Group Radio Access Network, Tech. Rep. 3GPP TR 37.977 V14.3.0, 2017.

[6] CTIA, "Test Plan for 2x2 Downlink MIMO and Transmit Diversity Over-the-Air Performance," Tech. Rep. Version 1.1.1, 2017.

[7] 3GPP, "Study on channel model for frequencies from 0.5 to 100 GHz," Tech. Rep. 3GPP TR 38.901 V14.0.0, 2017.

[8] WINNER, "WINNER II Channel Models: Part I Channel Models," Tech. Rep. D1.1.2 V1.2, 2007.

[9] B. H. Fleury, "First- and second-order characterization of direction dispersion and space selectivity in the radio channel," *IEEE Transactions on Information Theory*, vol. 46, no. 6, pp. 2027–2044, 2000.

[10] P. Bello, "Characterization of Randomly Time-Variant Linear Channels," *IEEE Transactions on Communications Systems*, vol. 11, no. 4, pp. 360–393, 1963.